Clin Orthop Relat Res (2013) 471:2422–2433
DOI 10.1007/s11999-013-2859-0

Clinical Orthopaedics and Related Research®
A Publication of The Association of Bone and Joint Surgeons®

SYMPOSIUM: NANOSCIENCE IN MUSCULOSKELETAL MEDICINE

Nano-ceramic Composite Scaffolds for Bioreactor-based Bone Engineering

Qing Lv PhD, Meng Deng PhD, Bret D. Ulery PhD, Lakshmi S. Nair M.Phil, PhD, Cato T. Laurencin MD, PhD

Published online: 22 February 2013

Abstract

Background Composites of biodegradable polymers and bioactive ceramics are candidates for tissue-engineered scaffolds that closely match the properties of bone. We previously developed a porous, three-dimensional poly (D,L-lactide-co-glycolide) (PLAGA)/nanohydroxyapatite (n-HA) scaffold as a potential bone tissue engineering matrix suitable for high-aspect ratio vessel (HARV) bioreactor applications. However, the physical and cellular properties of this scaffold are unknown. The present study aims to evaluate the effect of n-HA in modulating PLAGA scaffold properties and human mesenchymal stem cell (HMSC) responses in a HARV bioreactor.

Questions/purposes By comparing PLAGA/n-HA and PLAGA scaffolds, we asked whether incorporation of n-HA (1) accelerates scaffold degradation and compromises mechanical integrity; (2) promotes HMSC proliferation and differentiation; and (3) enhances HMSC mineralization when cultured in HARV bioreactors.

Methods PLAGA/n-HA scaffolds (total number = 48) were loaded into HARV bioreactors for 6 weeks and monitored for mass, molecular weight, mechanical, and morphological changes. HMSCs were seeded on PLAGA/n-HA scaffolds (total number = 38) and cultured in HARV bioreactors for 28 days. Cell migration, proliferation, osteogenic differentiation, and mineralization were characterized at four selected time points. The same amount of PLAGA scaffolds were used as controls.

Results The incorporation of n-HA did not alter the scaffold degradation pattern. PLAGA/n-HA scaffolds maintained their mechanical integrity throughout the 6 weeks in the dynamic culture environment. HMSCs seeded on PLAGA/n-HA scaffolds showed elevated proliferation, expression of osteogenic phenotypic markers, and mineral deposition as compared with cells seeded on PLAGA scaffolds. HMSCs migrated into the scaffold center with nearly uniform cell and extracellular matrix distribution in the scaffold interior.

Conclusions The combination of PLAGA/n-HA scaffolds with HMSCs in HARV bioreactors may allow for the generation of engineered bone tissue.

Clinical Relevance In cases of large bone voids (such as bone cancer), tissue-engineered constructs may provide alternatives to traditional bone grafts by culturing patients' own MSCs with PLAGA/n-HA scaffolds in a HARV culture system.

The institution of one or more of the authors (CTL) received funding from the National Science Foundation (Grant #BES0503207).
All ICMJE Conflict of Interest Forms for authors and *Clinical Orthopaedics and Related Research* editors and board members are on file with the publication and can be viewed on request.

Q. Lv, M. Deng, B. D. Ulery, L. S. Nair, C. T. Laurencin (✉)
Institute for Regenerative Engineering, University of Connecticut Health Center, Farmington, CT 06003, USA
e-mail: Laurencin@uchc.edu

Q. Lv, M. Deng, B. D. Ulery, L. S. Nair, C. T. Laurencin
Raymond and Beverly Sackler Center for Biological, Physical and Engineering Sciences, University of Connecticut Health Center, Farmington, CT, USA

M. Deng, B. D. Ulery, L. S. Nair, C. T. Laurencin
Department of Orthopaedic Surgery, University of Connecticut Health Center, Farmington, CT, USA

L. S. Nair, C. T. Laurencin
Department of Chemical, Materials and Biomolecular Engineering, University of Connecticut, Storrs, CT, USA

C. T. Laurencin
Connecticut Institute for Clinical and Translational Science, University of Connecticut, Farmington, CT, USA

Introduction

In the United States, it is estimated that one of every two Americans will experience a fracture before the age of 65 years [10]. For those patients with fractures treated surgically, 500,000 procedures annually involve the use of a bone graft [15]. With an increasingly aging population, this number will only continue to rise. Bone graft procedures have been conventionally accomplished using autografts and allografts. Although these grafts have led to clinically relevant healing, they possess disadvantages including limited supply, immune response induction, risk of disease transmission, and inconsistent bone healing. Studies have shown that the failure rate of allografts is between 25% and 35% [2, 35]. Bone tissue-engineered constructs using cells, scaffolds, and/or growth factors may provide an alternative strategy to traditional bone grafts [40].

Substantial prior bone tissue-engineering research has focused on the development of scaffolds that possess the proper material properties and pore structure necessary to fill bone defects [5, 34, 44]. Although a variety of bone graft substitute materials including metals, ceramics, and polymers have been used [24], polymer/ceramic composites possess a unique set of properties that allow them to best facilitate bone regeneration [20]. Biodegradable polymers like polyesters [12, 25, 53], poly(anhydride-co-imides) [1, 33], polyphosphazenes [21, 22], and polyurethanes [4, 30] are capable of providing initial mechanical structure and support for regenerating bone tissue, whereas bioactive ceramics such as hydroxyapatite [43, 50], tricalcium phosphate [18, 38], and octacalcium phosphate [31] possess intrinsic osteoinductivity that can induce desired bone cell differentiation. More specifically, porous three-dimensional (3-D) scaffolds composed of poly(D,L-lactide-co-glycolide) (PLAGA)/nanohydroxyapatite (n-HA) matrix enhance preosteoblast growth, differentiation, and mineralization [16, 39, 48].

Although in vitro results have been published in which cells are capable of penetrating the interior of polymer/ceramic scaffolds [24], these scaffolds alone are often only able to induce new bone tissue development in vivo at the scaffold surface [13, 27, 51]. This issue may be overcome by first cellularizing the scaffold with stem cells in vitro [17]. One cell source option is bone marrow mesenchymal stem cells (MSCs), which can differentiate into a variety of cells including osteoblasts, chondrocytes, and adipocytes [3]. Although MSCs represent a small fraction of marrow cells [52], they can be isolated, cryopreserved, and expanded [3] while still retaining their osteogenic potential making them an ideal cell source. However, cells may have difficulty migrating into the interior of these 3-D constructs. With static culture techniques, the transportation of oxygen, nutrients, and low-molecular-weight metabolites is limited by diffusion preventing cells from being able to survive in the scaffold interior. To overcome this problem, a variety of dynamic culture systems have been used including perfusion bioreactors [45, 56], spinner flasks [32, 58], roller bottles [26], and rotating wall bioreactors [55, 59]. The high-aspect ratio vessel (HARV) bioreactor is a low-shear, high-mass transfer system that improves cell-seeded bone tissue-engineering scaffold performance [6, 9, 60]. Although the HARV bioreactor has been used for the dynamic culturing of osteoblast [60] and preosteoblast cells [7, 11], it is unclear how human mesenchymal stem cells (HMSCs) behave in HARV bioreactors.

We therefore assessed whether incorporation of n-HA (1) accelerates scaffold degradation and compromises mechanical integrity; (2) promotes HMSC proliferation and differentiation; and (3) enhances HMSC mineralization when cultured in HARV bioreactors.

Materials and Methods

To answer the first key question, we conducted a dynamic degradation study of PLAGA/n-HA and PLAGA scaffolds in HARV bioreactors at 37 °C, in which scaffold weight, molecular weight, and surface morphology changes of the scaffolds were monitored over time (Fig. 1). The second study was carried out to answer the second and third questions. PLAGA/n-HA and PLAGA scaffolds were seeded with HMSCs and cultured in the HARV bioreactors for 28 days. At Days 7, 14, 21, and 28, samples were removed from bioreactors and DNA quantities, alkaline phosphatase (ALP) secretion, and calcium deposition were quantified and compared. The sample sizes were determined based on previously published results [7, 44, 60].

Cylindrical composite scaffolds (4 mm x 2.5 mm) with a PLAGA/n-HA ratio of 4:1 were fused at 90 °C for 3 hours as previously described [44]. We used cylindrical PLAGA scaffolds fused at 80 °C for 3 hours as controls.

We visualized the distribution of n-HA particles inside the microspheres and scaffolds by micro-CT. PLAGA/n-HA and PLAGA scaffolds were scanned by a micro-CT 40 machine (Scanco Medical AG, Basseersdorf, Switzerland) using a 12-mm sample holder, energy of 45 kV, current of 88 μA, and exposure time of 200 ms. Micro-CT analysis confirmed that the n-HA particles (red) were present within the composite scaffolds (Fig. 2).

Dynamic degradation of PLAGA/n-HA and PLAGA scaffolds was conducted in HARV bioreactors at 37 °C. HARV bioreactors were filled with 55 mL phosphate-buffered saline (PBS; pH = 7.4) and rotated at 35 rpm. PLAGA/n-HA (48 total) and PLAGA (48 total) scaffolds were loaded into two bioreactors and rotated continuously for a total of 6 weeks. Each week we removed eight

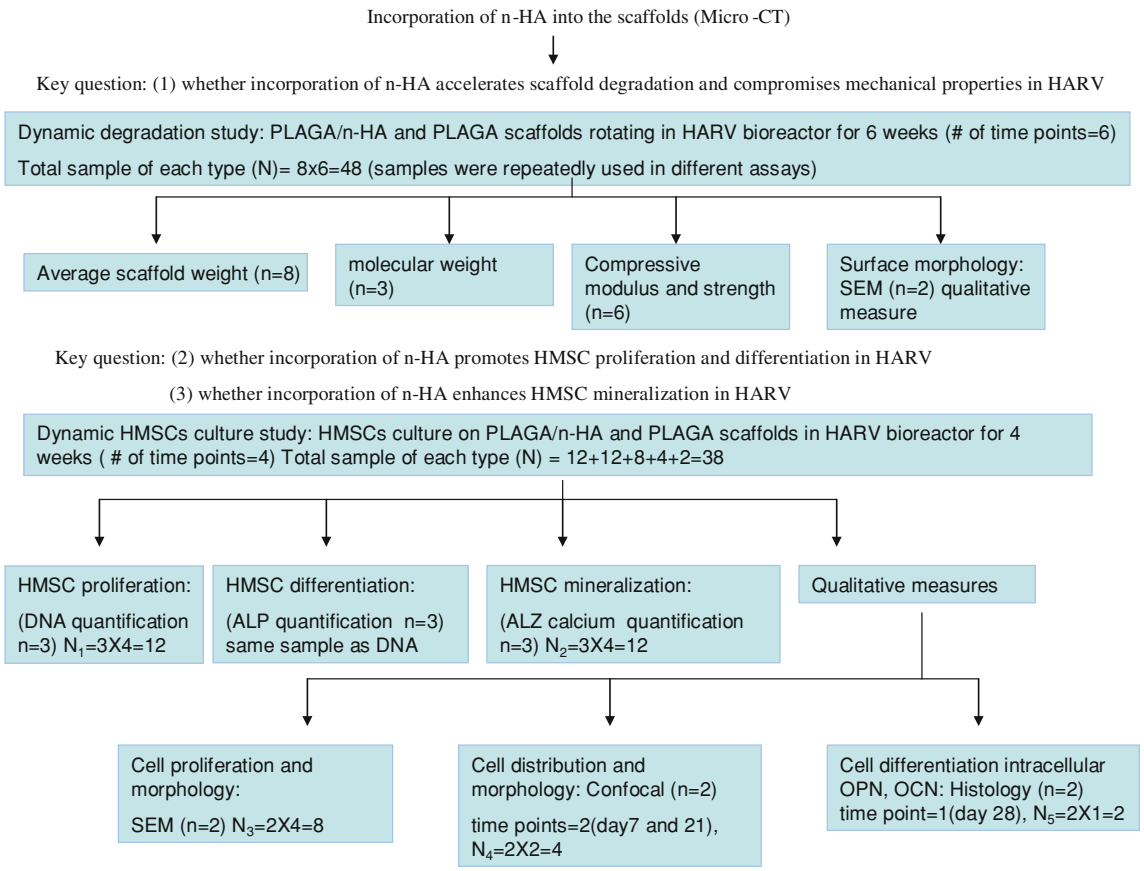

Fig. 1 A flowchart illustrates the experimental design of the study.

samples of each kind from the bioreactors and dried them for weight determination, mechanical testing, molecular weight analysis, and scanning electron microscopy (SEM). We weighed all scaffolds individually before the degradation study. Each week, random samples (n = 8) were taken out of the bioreactor and the average scaffold weight for both composite and polymeric scaffolds were determined. Because the samples were taken randomly from the bioreactors, their original weights before degradation were not known. Therefore, we compared the average weight at each time point with the original average scaffold weight before degradation.

We evaluated compressive modulus and strength changes resulting from degradation on a weekly basis. After weight measurements, six of the eight fully dried scaffolds were subjected to compression test using an Instron mechanical testing machine (Instron Model 5544, Canton, MA, USA) at a crosshead speed of 5 mm/min at ambient temperature and humidity. We determined compressive modulus and maximum compressive strength of scaffolds using Merlin software (Instron, Norwood, MA, USA) associated with the Instron machine.

We evaluated the polymer molecular weight of both composite scaffolds and pure polymeric scaffolds on a weekly basis during the degradation study. After mechanical testing, three of the six scaffolds were dissolved in THF to form 0.1% polymer solutions and then centrifuged at 5000 rpm for 10 minutes. The supernatant polymer solution was carefully removed without disturbing the n-HA pellet and filtered through 0.45-μm filters. Molecular weight analysis was carried out using gel permeation chromatography (GPC). The GPC system consists of a Waters 717 plus Autosampler (Water Corporation, Milford, MA, USA), a Waters 2414 Refractive Index Detector, a Waters 2487 Dual λ Absorbance detector, and a Polymer Labs (Varian Inc, Amherst, MA, USA) ELSD 1000 Detector. We used a series of four JORDI DVB divinyl benzene flash columns (Jordi Lab, Mansfield, MA, USA). The system operates with a mobile phase of THF at a flow rate of 2 mL/min at 40° C and an injection volume of 100 μL. The weight average molecular weight was calculated using Millennium®32 software (Water Corporation, Milford, MA, USA).

The changes in scaffold surface morphology during degradation were monitored by SEM. In brief, fully dried scaffolds were sputtercoated with gold/palladium and examined with a HITACHI TM-1000 (Hitachi High

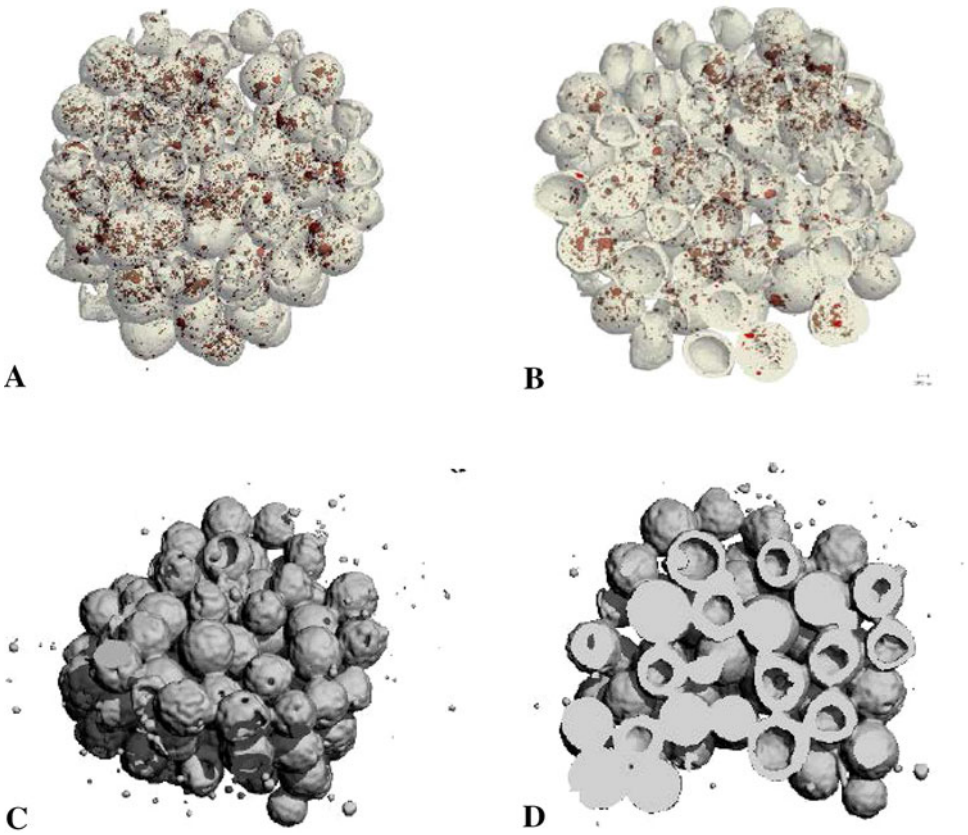

Fig. 2A–D Three-dimensional (3-D) micro-CT reconstructions of PLAGA/n-HA (**A**–**B**) and PLAGA (**C**–**D**) scaffolds at the surface (**A**, **C**) and cross-sectional interior (**B**, **D**). Red dots represent n-HA.

Technologies America Inc, Pleasanton, CA, USA) tabletop microscope. Four of the authors examined the SEM images and each picture represents the typical case in at least three different areas.

We purchased HMSCs from Lonza Walkersville Inc (Walkersville, MD, USA). The cells were expanded and maintained in Mesenchymal Stem Cell Basal Medium purchased from Lonza. Scaffolds were soaked in 70% ethanol for 15 minutes, washed with sterile water twice for 15 minutes each time, and further sterilized by ultraviolet irradiation for 30 minutes on each side. HMSCs (Passage 4) were seeded onto 38 PLAGA/n-HA scaffolds and 38 PLAGA scaffolds at a density of 5 x 10^4 cells/scaffold. After 24 hours, the scaffolds were transferred into 50-mL HARV bioreactors rotating at 35 rpm and cultured in osteogenic media (Lonza) at 37 °C and 5% CO_2. At Days 7, 14, 21, and 28, we removed scaffolds from the bioreactor for characterization.

Cell proliferation was quantified by measuring the DNA content of the cells. At predetermined time points, we removed three scaffolds of each type from the bioreactor, washed them with PBS, and transferred them into 48-well plates. Cells were lysed with 1 mL 1% Triton X-100 solution and then subjected to three freeze-thaw cycles. We stored the resultant cell lysates at −70° C for further assay. At the end of the culture period, the cell lysate samples were thawed together and assayed using a PicoGreen® double-stranded DNA(dsDNA) Quantification kit (Molecular Probes, Eugene, OR, USA).

To visualize HMSC morphology and distribution on the scaffold surface by SEM, cell-seeded scaffolds were fixed at 4 °C in 1% glutaraldehyde for 1 hour and then in 3% glutaraldehyde for 24 hours. The scaffolds were dehydrated sequentially for 10 minutes each using an ethanol series (30%, 50%, 70%, 80%, 90%, 95%, and 100%). Scaffolds were allowed to dry overnight, coated with gold/palladium, and viewed by SEM (JEOL 6700, Tokyo, Japan) at an acceleration voltage of 3 kV.

We measured ALP activity, an early marker of osteoblast activity, using an ALP substrate kit (Bio-Rad, Hercules, CA, USA). The same cell lysates collected for cell proliferation were used for this assay.

Mineralization was characterized by calcium quantification using an Alizarin red staining assay. In brief, we removed three scaffolds of each type from the bioreactors at predetermined time points and washed them with PBS. Scaffolds were fixed with 70% ethanol at 4 °C for 1 hour and stained with 10% Alizarin red (Sigma, St Louis, MO, USA) solution for 10 minutes. The scaffolds were then washed with deionized water five or more times until the wash no longer showed presence of nonadsorbed stain. We took pictures of stained scaffolds with a stereo microscope

(Discovery V12; Zeiss, Thornwood, NY, USA). Next, 1 mL 10% cetylpyridinium chloride (Sigma-Aldrich) solution was added to each scaffold to dissolve the absorbed stain. The optical density of the solution was read spectrophotometrically (TECAN, Männedorf, Switzerland) at 550 nm.

We further visualized HMSC distribution on scaffolds by immunofluorescent staining for cell nuclei and cytoskeletal protein actin under a Zeiss LSM 510 UV confocal laser scanning microscope (Carl Zeiss MicroImaging Inc, Thornwood, NY, USA). The nuclei and actin fibers were stained by DAPI and TRITC-conjugated phalloidin (CHEMICON International Inc, Temecular, CA, USA), respectively. We visualized the nuclei and actin fiber stains under different light sources and these are shown in blue and red, respectively.

Histological analysis and immunostaining were used to visualize cell migration, tissue formation, and extracellular protein deposition in the scaffolds. We removed two HMSC-seeded scaffolds of each kind from the bioreactor at the end of the culture period, washed them with PBS, and then fixed them in 10% formalin at room temperature for 1 week. The samples were decalcified in a commercial product, Cal-Ex (Fisher Scientific), which contains HCl

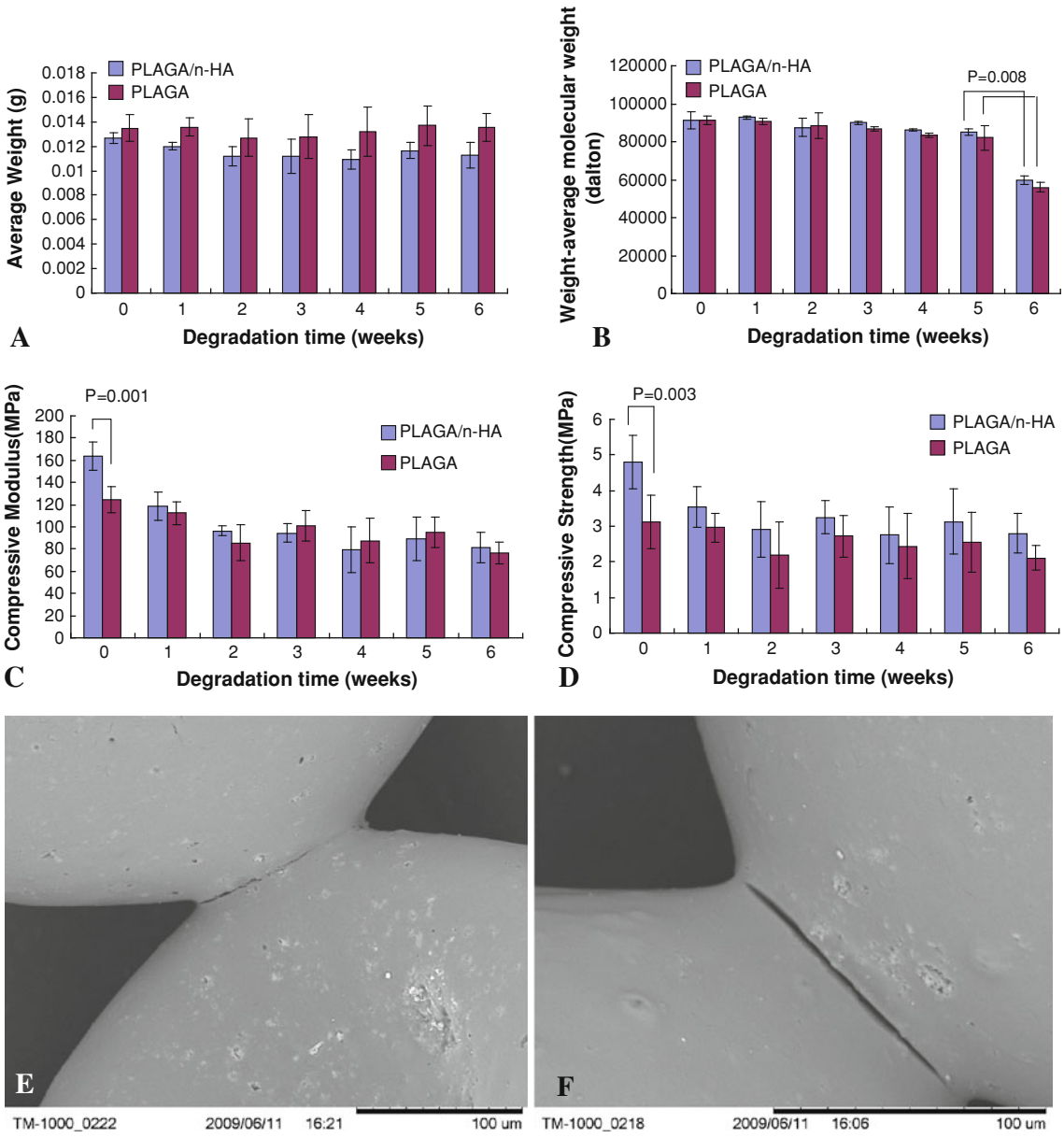

Fig. 3A–F PLAGA/n-HA and PLAGA scaffold degradation under dynamic conditions. (**A**) Average scaffold weight and (**B**) PLAGA weight-average molecular weight change over time. (**C**) Scaffold compressive modulus and (**D**) compressive strength change over time. Scanning electron micrographs of PLAGA/n-HA scaffolds at (**E**) 3 weeks and (**F**) 6 weeks.

and EDTA and then embedded them in a paraffin block. Five-micron-thick sections were cut from three different depths of the block and mounted on poly-L-lysine-coated slides. We removed the paraffin by toluene and the samples were rehydrated through graded alcohols to distilled water. The slides were subjected to different types of stains: hematoxylin and eosin (H&E) stain, osteopontin (OPN) immunostain, and osteocalcin (OCN) immunostain. The stained slices were analyzed qualitatively by light microscopy by three of the authors (QL, MD, LSN). Both PLAGA and PLAGA/n-HA scaffolds were dissolved during histological processing. Cell-seeded scaffolds before osteogenic induction were used as negative controls and also found to be completely dissolved. For the cell-seeded PLAGA group after osteogenic induction, there was not enough cell/tissue formation to be observed and analyzed under the microscope.

One-way analysis of variance and Tukey's test were performed to determine statistical differences in mechanical and cellular properties between different scaffold types and different time points. We performed statistical analysis using XLSTAT Pro 7.5 software (Addinsoft, New York, NY, USA). Error bars indicate SD.

Results

The average weight of both PLAGA/n-HA and PLAGA scaffolds showed no changes over the 6 weeks of the study (Fig. 3A) indicating the incorporation of n-HA did not change the scaffold erosion pattern. Scaffold polymer molecular weight stayed relatively unchanged for the first 5 weeks of dynamic culture (Fig. 3B). Between 5 and 6 weeks, the molecular weight of both scaffold types decreased ($p = 0.008$). PLAGA/n-HA scaffolds showed higher compressive moduli ($p = 0.001$) and compressive strengths ($p = 0.003$) than PLAGA scaffolds at Week 0 (Fig. 3C–D). During initial degradation, the PLAGA scaffolds showed no change in mechanical properties, whereas the PLAGA/n-HA scaffolds showed a decrease ($p = 0.001$) in compressive moduli. At 6 weeks, we observed no difference in mechanical properties between the two scaffold types. SEMs illustrate occasional cracks were formed between neighboring microspheres on the surface of PLAGA/n-HA scaffolds after 3 weeks (Fig. 3E). Larger cracks were seen on the scaffold surface at 6 weeks (Fig. 3F).

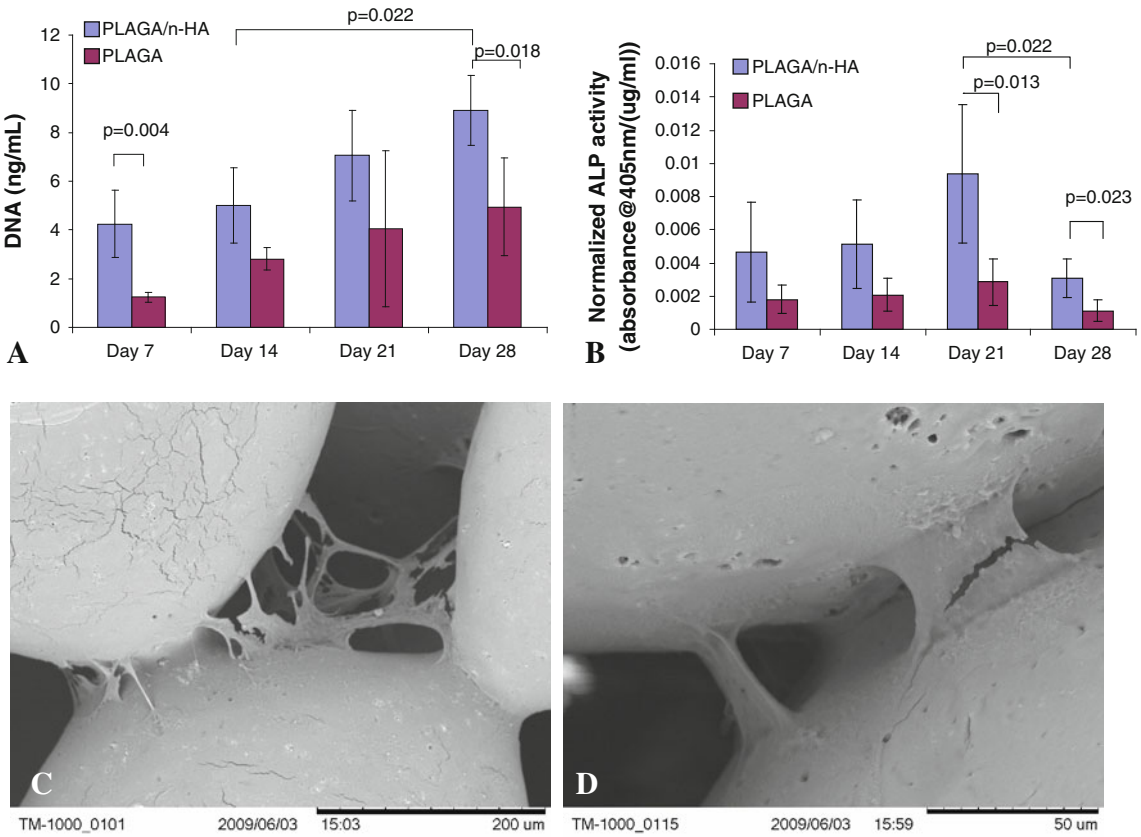

Fig. 4A–D (**A**) Cell proliferation over time as measured by DNA quantification. (**B**) Normalized ALP activity of cells seeded on scaffolds over time. SEMs of cells on the surface of PLAGA/n-HA scaffolds at Day 14 (**C**) and Day 28 (**D**).

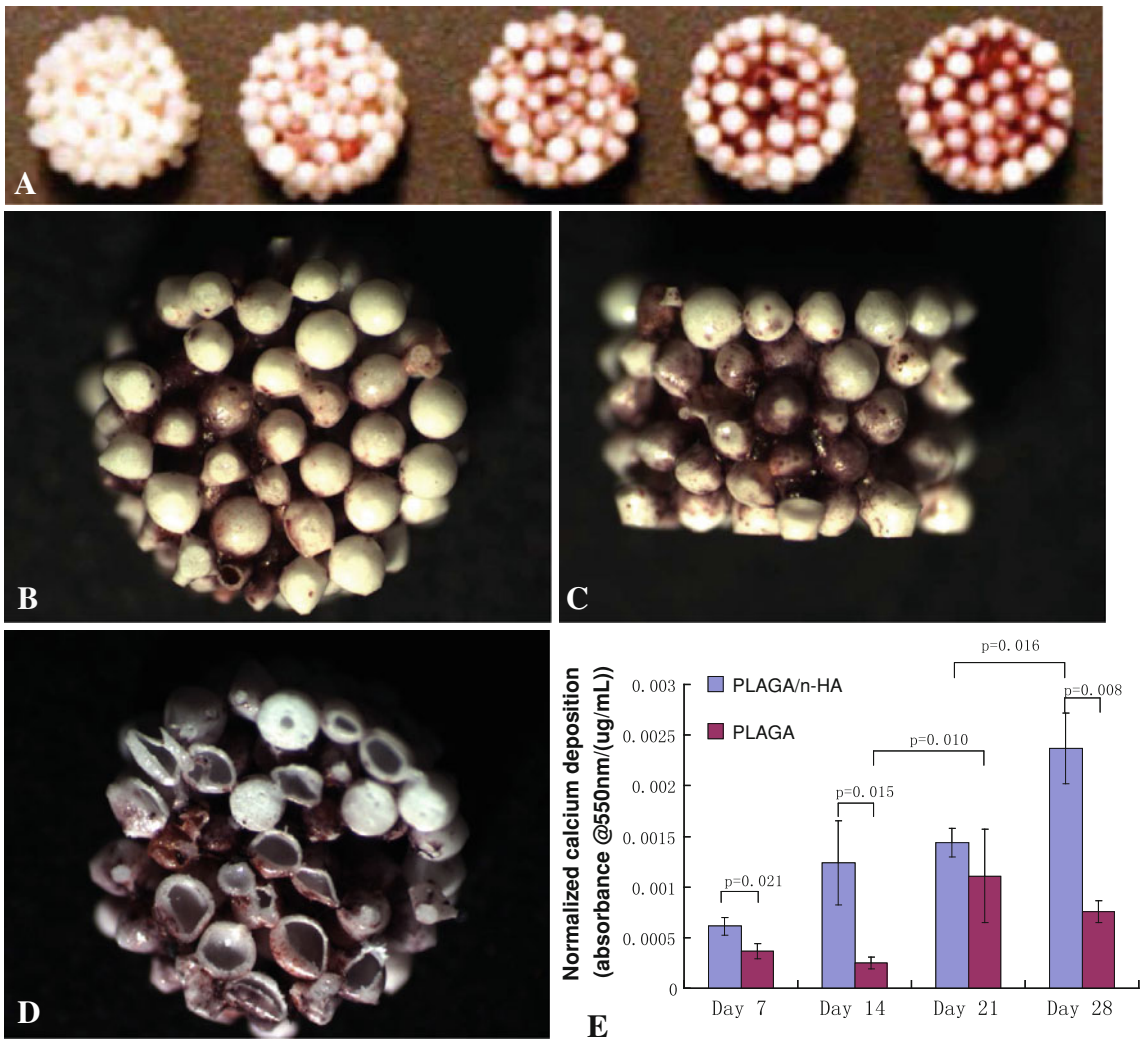

Fig. 5A–E Calcium deposition by HMSCs over time. (**A**) Alizarin red staining of PLAGA/n-HA scaffolds: blank scaffold without cells and scaffolds seeded with cells for 7, 14, 21, and 28 days (left to right). SEM images of the (**B**) end, (**C**) side, and (**D**) cross-sectional interior of Alizarin red-stained cell-seeded PLAGA/n-HA scaffolds at Day 21. (**E**) Desorbed Alizarin red quantification as measured spectrophotometrically at 550 nm.

HMSCs seeded on PLAGA/n-HA scaffolds cultured in HARV bioreactors showed increased DNA quantity ($p = 0.022$) with culture time indicating normal cell growth (Fig. 4A). At Day 28, DNA quantity was higher ($p = 0.018$) for HMSCs on PLAGA/n-HA scaffolds than on PLAGA scaffolds. ALP activity for HMSCs cultured on PLAGA/n-HA scaffolds showed an increasing trend with culture time until Day 21 and dropping ($p = 0.022$) at Day 28 (Fig. 4B). A similar trend was observed for HMSCs cultured on PLAGA scaffolds; however, there was no difference among any of the time points. At Days 21 and 28, ALP activity of HMSCs cultured on PLAGA/n-HA scaffolds was higher ($p = 0.013$ on Day 21 and $p = 0.023$ on Day 28) than HMSCs cultured on PLAGA scaffolds. SEM showed that HMSCs were mainly located at the adjoining area between neighboring microspheres on PLAGA/n-HA scaffolds (Fig. 4C–D).

With increasing culture time we qualitatively observed a deeper red color suggesting increased Alizarin red deposition on PLAGA/n-HA scaffolds (Fig. 5A). From the end view of a PLAGA/n-HA scaffold (Fig. 5B), the exterior layer of microspheres remained mostly unstained. However, we observed areas of dark red stain in between the microspheres. From a side view of a PLAGA/n-HA scaffold (Fig. 5C), the center of the scaffold appeared more heavily stained than the outside of the scaffold. When stained scaffolds were cut open, heavy Alizarin red staining was found at the center of the scaffold (Fig. 5D). On Day 7, HMSC nuclei were loosely located near the adjoining areas of microspheres (Fig. 6A). Actin fibers were not abundant

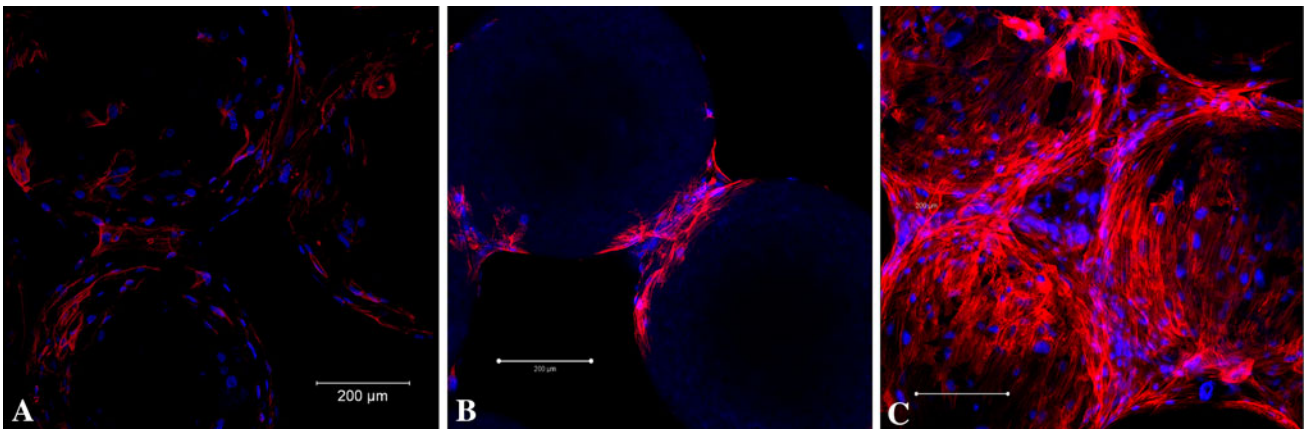

Fig. 6A–C Immunofluorescent staining of HMSCs on PLAGA/n-HA scaffolds with DAPI (cell nuclei) and TRITC-conjugated phalloidin (polymerized actin) at (**A**) Day 7 (scaffold surface), (**B**) Day 21 (scaffold surface), and (**C**) Day 21 (scaffold center). The scale bars represent 200 µm.

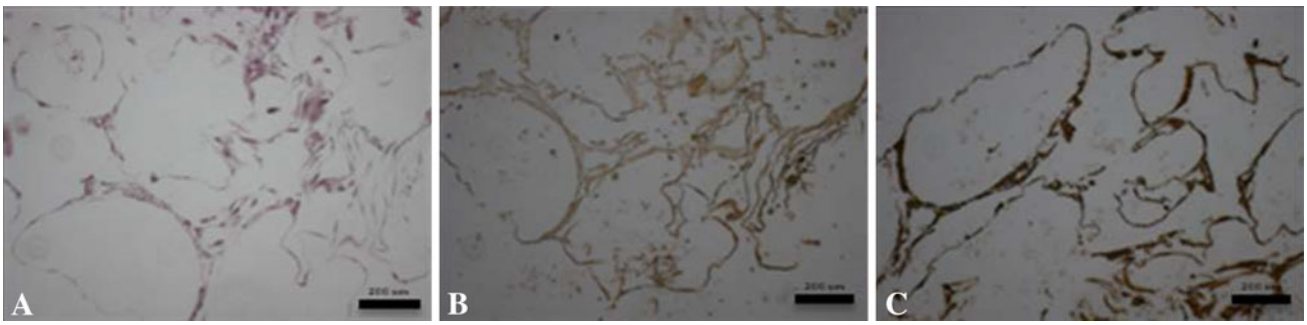

Fig. 7A–C After 28 days of dynamic culturing in a HARV bioreactor, HMSC-seeded PLAGA/n-HA scaffolds were stained with (**A**) H&E, (**B**) osteocalcin immunostain, or (**C**) osteopontin immunostain. Each image is representative of three different levels of three independent samples. The scale bars represent 200 µm.

and exhibited random-oriented fiber morphology. We found HMSCs mainly at the adjoining area between microspheres on the surface of PLAGA/n-HA scaffolds at Day 21 (Fig. 6 B). However, at the center of PLAGA/n-HA scaffolds (Fig. 6C), HMSCs appeared to have proliferated and covered the entire surface of the microspheres. Spectrophotometrically quantified desorbed Alizarin red stain increased ($p = 0.016$ for PLAGA/n-HA and $p = 0.010$ for PLAGA) over time (Fig. 5E) indicating greater calcium deposition for both scaffold types. At Days 7, 14, and 28, a greater quantity ($p = 0.021$, $p = 0.015$, and $p = 0.008$, respectively) of Alizarin red stain was detected for PLAGA/n-HA scaffolds than for PLAGA scaffolds. H&E-stained histological sections from different depth levels inside the PLAGA/n-HA scaffolds confirmed that HMSCs were present throughout the scaffold interior (Fig. 7A). We detected extracellular OCN (Fig. 7B) and OPN (Fig. 7C) at different locations of the scaffold interior providing evidence that HMSCs not only migrated into the interior of the scaffold, but also differentiated and maturated into osteogenic cells. These findings corroborate the qualitative ALZ results.

Discussion

The design of an ideal bone regenerative engineering strategy necessitates the fundamental investigation into the roles that scaffold properties and culture environment play in modulating stem cell responses such as cell migration, proliferation, differentiation, and mineralization. In our previous in vitro work under static conditions, we found the PLAGA/n-HA composite system supports elevated expression of phenotypic markers such as ALP as well as mineral deposition of HMSCs [44]. We therefore asked whether incorporation of n-HA would (1) accelerate scaffold degradation and compromise mechanical integrity; (2) promote HMSC proliferation and differentiation; and (3) enhance HMSC mineralization when cultured in HARV bioreactors.

The current study presents a few limitations to be considered. First, as a result of the limited number of HARV bioreactors in our laboratory, the scaffold weight change during degradation was based on the average weight of random samples. Given the similar dimension and weight

of the samples within the bioreactor, the average weight change was the closest approximation of the direct weight change of each specific sample. Second, the enhanced differentiation of HMSCs was demonstrated through measurements of phenotypic markers. The underlying molecular signaling pathway governing the cell-scaffold interactions and promotion of osteogenic differentiation in the dynamic culture environment requires further focused efforts. Third, static culture was not included because the benefits of HARV bioreactor culture as compared with the static culture have been established previously and the aim of this study was to investigate the effect of n-HA on HMSC behavior in the bioreactor. Fourth, in the control group there was not enough tissue formation to be shown in the histological analysis during the 28 days of culture period. A future cell study with a longer culture period would help reveal the cell and tissue growth inside the PLAGA scaffolds.

The extent of flow in the physiological environment makes a dynamic degradation study more representative. To our knowledge, there are no dynamic degradation studies of PLAGA or PLAGA composite in HARV bioreactors so far. Our data demonstrated that the introduction of n-HA resulted in a marked difference in scaffold mechanical integrity despite no changes in the polymer erosion pattern. Before degradation, the PLAGA/n-HA scaffolds exhibited higher mechanical properties than PLAGA scaffolds. At early time points, a more pronounced decrease in compressive modulus and strength of PLAGA/n-HA was observed as compared with PLAGA scaffolds. The mechanical properties of sintered polymer microsphere scaffolds largely depend on the fusion area between neighboring microspheres [5, 37]. The process of PLAGA degradation starts with water intake [23, 57]. The hydrophilic nature of HA may increase the extent of water attack at the adjoining area between neighboring microspheres, therefore causing the crack formation, which deteriorated the mechanical properties of scaffolds (Fig. 3E–F). Hydrolysis generates low-molecular-weight oligomers, which do not diffuse out the polymer matrix immediately. Thus, polymer M_w decreases but average weights of samples remain constant and the 3-D structures remain intact. It has been reported that these entrapped oligomers with more carboxylic chain ends can further autocatalyze ester bond hydrolysis [57]. The soluble degraded oligomers near the surface are easier to leach out into surrounding media. In contrast, the oligomers deep inside the polymer matrix tend to accumulate, which causes greater autocatalysis locally [57]. The abrupt decrease in M_w at the sixth week expedited the degradation rate as compared with rates in the previous 5 weeks, which may be caused by the autocatalysis.

Calcium phosphate ceramics, especially HA, are bioactive materials capable of promoting osteogenesis of MSCs [14, 47]. Substrate topography comprised of various micro- and nanofeatures influences cellular behavior [46]. Dalby et al. [19] showed that random circular nanostructures with a diameter of approximately 120 nm promoted and directed osteogenic differentiation of HMSCs in the absence of osteogenic supplements in cell culture media, suggesting that nanofeatures alone can stimulate osteogenic differentiation and mineral production in vitro. Various composite scaffolds containing n-HA have been developed with favorable osteogenic responses [36, 41, 61]. For the PLAGA/n-HA scaffolds used in this study, the n-HA nanoparticles incorporated into the microsphere surface had an average size of 100 nm providing a nanotopographical feature that may be beneficial to HMSC growth and differentiation [19]. During in vitro static culture, HMSCs showed greater proliferation on PLAGA/n-HA scaffolds than on PLAGA scaffolds. Furthermore, HMSCs seeded on PLAGA/n-HA scaffolds showed elevated expression of osteogenic phenotypic markers compared with cells seeded on PLAGA scaffolds. Such enhanced HMSC response to the composites further corroborated our previous findings under static conditions [44]. For example, ALP activity reportedly indicates the commitment of MSCs toward the osteoblastic lineage at early differentiation stages [42]. PLAGA/n-HA scaffolds supported enhanced HMSC ALP expression on Days 21 and 28 as compared with PLAGA scaffolds, indicating promoted osteoblastic differentiation. ALP expression increased with culture time peaking at Day 21. On Day 28, the ALP expression decreased from its maximal value. Rat marrow stromal cells cultured in spinner flasks showed peak ALP expression on Day 14 and ALP activity decreased when cell culture was extended to Day 21 [54]. MSCs of different species might exhibit peak marker expression at different times; however, the general pattern of production is relatively conserved because it is related to each marker's function. ALP usually reaches a maximum that coincides with early osteoblastic differentiation and decreases afterward when matrix maturation and mineralization begin [28]. Additionally, OCN and OPN characterization by enzyme-linked immunosorbent assay further confirmed the osteoblastic differentiation state of HMSCs (data not shown). The HMSC behavior on scaffolds in the dynamic culture environment may also be influenced by shear force [29]. In the HARV bioreactor, the theoretical value of generated shear stress has been estimated to be 0.16 to 0.32 N/m^2, which was sufficient enough to induce enhanced osteoblast differentiation [8, 60]. In the current work, we found this range of shear suitable for HMSC growth and differentiation on PLAGA/n-HA scaffolds.

As an indication of osteoblastic differentiation and maturation, calcium deposition by HMSCs was increased on PLAGA/n-HA scaffolds than on PLAGA scaffolds. Notably, more pronounced mineralization was found in the

scaffold interior than on the scaffold surfaces. This finding is in contrast to static cultured tissue-engineered constructs in which cell ingress into the interior is reportedly limited to a depth of several hundred microns [13, 27, 49, 51]. Further actin and nucleus staining of HMSCs on PLAGA/n-HA scaffolds suggested a greater number of cells were distributed uniformly in the interior of scaffolds than on the surface of scaffolds (Fig. 6). Additionally, histological staining at different depths of the scaffolds revealed a network of cells and extracellular OPN and OCN throughout the 3-D scaffold structure (Fig. 7). These findings suggest the nutrient transport and waste removal in HARV bioreactors were efficient enough to allow cells to migrate into the scaffold center. The difference in shear stresses experienced between cells on the surface and cells in the center of the scaffold might explain the observation of more abundant cells in the scaffold interior [6, 8].

In summary, we found HMSCs seeded on PLAGA/n-HA scaffolds and cultured in HARV bioreactors were well distributed throughout the 3-D structure of the scaffolds and exhibited desirable proliferation, differentiation, and mineralization behavior. Such enhanced performance of HMSCs can be attributed to scaffolding materials, structure, surface nanotopography as well as the culture environment. Therefore, in vitro culture of HMSCs on PLAGA/n-HA scaffolds in HARV bioreactors holds great potential in the development of alternative grafts to repair and regenerate bone.

Acknowledgments We thank Ms Jan Redick from Advanced Microscopy Facility at the School of Medicine of the University of Virginia for her assistance in confocal imaging. We thank Dr Liisa Kuhn from the Department of Reconstructive Sciences at the University of Connecticut Health Center (UCHC) for allowing us to use their SEM. We also thank Dr Douglas Adams from the Department of Orthopaedic Surgery at UCHC for help with micro-CT analysis.

References

1. Attawia MA, Herbert KM, Uhrich KE, Langer R, Laurencin CT. Proliferation, morphology, and protein expression by osteoblasts cultured on poly(anhydride-co-imides). *J Biomed Mater Res.* 1999;48:322–327.
2. Berrey B, Lord C, Gebhardt M, Mankin H. Fractures of allografts. Frequency, treatment, and end-results. *J Bone Joint Surg Am.* 1990;72:825–833.
3. Bianco P, Riminucci M, Gronthos S, Robey PG. Bone marrow stromal stem cells: nature, biology, and potential applications. *Stem Cells.* 2001;19:180–192.
4. Bil M, Ryszkowska J, Woźniak P, Kurzydłowski KJ, Lewandowska-Szumieł M. Optimization of the structure of polyurethanes for bone tissue engineering applications. *Acta Biomaterialia.* 2010;6:2501–2510.
5. Borden M, El-Amin SF, Attawia M, Laurencin CT. Structural and human cellular assessment of a novel microsphere-based tissue engineered scaffold for bone repair. *Biomaterials.* 2003;24:597–609.
6. Botchwey EA, Dupree MA, Pollack SR, Levine EM, Laurencin CT. Tissue engineered bone: Measurement of nutrient transport in three-dimensional matrices. *J Biomed Mater Res A.* 2003;67:357–367.
7. Botchwey EA, Pollack SR, El-Amin S, Levine EM, Tuan RS, Laurencin CT. Human osteoblast-like cells in three-dimensional culture with fluid flow. *Biorheology.* 2003;40:299–306.
8. Botchwey EA, Pollack SR, Levine EM, Johnston ED, Laurencin CT. Quantitative analysis of three-dimensional fluid flow in rotating bioreactors for tissue engineering. *J Biomed Mater Res A.* 2004;69:205–215.
9. Botchwey EA, Pollack SR, Levine EM, Laurencin CT. Bone tissue engineering in a rotating bioreactor using a microcarrier matrix system. *J Biomed Mater Res.* 2001;55:242–253.
10. Brinker MR, O'Connor DP. The incidence of fractures and dislocations referred for orthopaedic services in a capitated population. *J Bone Joint Surg Am.* 2004;86:290–297.
11. Bucaro M, Fertala J, Adams C, Steinbeck M, Ayyaswamy P, Mukundakrishnan K, Shapiro I, Risbud M. Bone cell survival in microgravity: evidence that modeled microgravity increases osteoblast sensitivity to apoptogens. *Ann NY Acad Sci.* 2004;1027:64–73.
12. Cai YZ, Zhang GR, Wang LL, Jiang YZ, Ouyang HW, Zou XH. Novel biodegradable three-dimensional macroporous scaffold using aligned electrospun nanofibrous yarns for bone tissue engineering. *J Biomed Mater Res A.* 2012;100:1187–1194.
13. Cai Z, Zhang T, Di L, Xu DM, Xu DH, Yang DA. Morphological and histological analysis on the *in vivo* degradation of poly (propylene fumarate)/(calcium sulfate/β-tricalcium phosphate). *Biomed Microdevices.* 2011;13:623–631.
14. Chai YC, Roberts SJ, Schrooten J, Luyten FP. Probing the osteoinductive effect of calcium phosphate by using an in vitro biomimetic model. *Tissue Eng Part A.* 2010;17:1083–1097.
15. Cheung C. The future of bone healing. *Clin Podiatr Med Surg.* 2005;22:631.
16. Choi SW, Zhang Y, Thomopoulos S, Xia Y. In vitro mineralization by preosteoblasts in poly(DL-lactide-co-glycolide) inverse opal scaffolds reinforced with hydroxyapatite nanoparticles. *Langmuir.* 2010;26:12126–12131.
17. Ciapetti G, Granchi D, Baldini N. The combined use of mesenchymal stromal cells and scaffolds for bone repair. *Curr Pharm Des.* 2012;18:1796–1820.
18. Clarke S, Hoskins N, Jordan G, Marsh D. Healing of an ulnar defect using a proprietary TCP bone graft substitute, JAX' in association with autologous osteogenic cells and growth factors. *Bone.* 2007;40:939–947.
19. Dalby MJ, Gadegaard N, Tare R, Andar A, Riehle MO, Herzyk P, Wilkinson CDW, Oreffo ROC. The control of human mesenchymal cell differentiation using nanoscale symmetry and disorder. *Nat Mater.* 2007;6:997–1003.
20. Deng M, Kumbar SG, Lo KWH, Ulery BD, Laurencin CT. Novel polymer-ceramics for bone repair and regeneration. *Recent Pat Biomed Eng.* 2011;4:168–184.
21. Deng M, Kumbar SG, Nair LS, Weikel AL, Allcock HR, Laurencin CT. Biomimetic structures: biological implications of dipeptide-substituted polyphosphazene-polyester blend nanofiber matrices for load-bearing bone regeneration. *Adv Funct Mater.* 2011;21:2641–2651.
22. Deng M, Kumbar SG, Wan Y, Toti US, Allcock HR, Laurencin CT. Polyphosphazene polymers for tissue engineering: an analysis of material synthesis, characterization and applications. *Soft Matter.* 2010;6:3119–3132.
23. Deng M, Nair LS, Nukavarapu SP, Kumbar SG, Jiang T, Weikel AL, Krogman NR, Allcock HR, Laurencin CT. In situ porous structures: a unique polymer erosion mechanism in biodegradable dipeptide-based polyphosphazene and polyester blends producing matrices for regenerative engineering. *Adv Funct Mater.* 2010;20:2794–2806.

24. Dinopoulos H, Dimitriou R, Giannoudis PV. Bone graft substitutes: what are the options? *Surgeon.* 2012;10:230–239.
25. El-Amin S, Lu H, Khan Y, Burems J, Mitchell J, Tuan R, Laurencin C. Extracellular matrix production by human osteoblasts cultured on biodegradable polymers applicable for tissue engineering. *Biomaterials.* 2003;24:1213–1221.
26. Emani S, Mayer JE Jr, Emani SM. Gene regulation of extracellular matrix remodeling in human bone marrow stem cell-seeded tissue-engineered grafts. *Tissue Eng A.* 2011;17:2379–2388.
27. Erdemli O, Captug O, Bilgili H, Orhan D, Tezcaner A, Keskin D. In vitro and in vivo evaluation of the effects of demineralized bone matrix or calcium sulfate addition to polycaprolactone-bioglass composites. *J Mater Sci Mat Med.* 2010;21:295–308.
28. Gomes ME, Sikavitsas VI, Behravesh E, Reis RL, Mikos AG. Effect of flow perfusion on the osteogenic differentiation of bone marrow stromal cells cultured on starch-based three-dimensional scaffolds. *J Biomed Mater Res A.* 2003;67:87–95.
29. Grellier M, Bareille R, Bourget C, Amédée J. Responsiveness of human bone marrow stromal cells to shear stress. *J Tissue Eng Regen Med.* 2009;3:302–309.
30. Guelcher SA, Brown KV, Li B, Guda T, Lee BH, Wenke JC. Dual-purpose bone grafts improve healing and reduce infection. *J Orthop Trauma.* 2011;25:477–482.
31. Habibovic P, Van der Valk C, Van Blitterswijk C, De Groot K, Meijer G. Influence of octacalcium phosphate coating on osteoinductive properties of biomaterials. *J Mater Sci Mater Med.* 2004;15:373–380.
32. He W, Nieponice A, Soletti L, Hong Y, Gharaibeh B, Crisan M. Pericyte-based human tissue engineered vascular grafts. *Biomaterials.* 2010;31:8235–8244.
33. Ibim SEM, Uhrich KE, Attawia M, Shastri VR, El-Amin SF, Bronson R, Langer R, Laurencin CT. Preliminary *in vivo* report on the osteocompatibility of poly(anhydride-co-imides) evaluated in a tibial model. *J Biomed Mater Res.* 1998;43:374–379.
34. Ishaug SL, Crane GM, Miller MJ, Yasko AW, Yaszemski MJ, Mikos AG. Bone formation by three-dimensional stromal osteoblast culture in biodegradable polymer scaffolds. *J Biomed Mater Res.* 1997;36:17–28.
35. Ito H, Koefoed M, Tiyapatanaputi P, Gromov K, Goater JJ, Carmouche J, Zhang X, Rubery PT, Rabinowitz J, Samulski RJ, Nakamura T, Soballe K, O'Keefe RJ, Boyce BF, Schwarz EM. Remodeling of cortical bone allografts mediated by adherent rAAV-RANKL and VEGF gene therapy. *Nat Med.* 2005;11:291–297.
36. Jiang L, Li Y, Xiong C. Preparation and biological properties of a novel composite scaffold of nano-hydroxyapatite/chitosan/carboxymethyl cellulose for bone tissue engineering. *J Biomed Sci.* 2009;16:65.
37. Jiang T, Abdel-Fattah WI, Laurencin CT. *In vitro* evaluation of chitosan/poly(lactic acid-glycolic acid) sintered microsphere scaffolds for bone tissue engineering. *Biomaterials.* 2006;27:4894–4903.
38. Kondo N, Ogose A, Tokunaga K, Umezu H, Arai K, Kudo N, Hoshino M, Inoue H, Irie H, Kuroda K. Osteoinduction with highly purified beta-tricalcium phosphate in dog dorsal muscles and the proliferation of osteoclasts before heterotopic bone formation. *Biomaterials.* 2006;27:4419–4427.
39. Lao L, Wang Y, Zhu Y, Zhang Y, Gao C. Poly (lactide-co-glycolide)/hydroxyapatite nanofibrous scaffolds fabricated by electrospinning for bone tissue engineering. *J Mater Sci Mater Med.* 2011;22:1873–1884.
40. Laurencin CT, Ambrosio AMA, Borden MD, Cooper JA. Tissue engineering: orthopedic applications. *Annu Rev Biomed Eng.* 1999;1:19–46.
41. Lee JH, Rim NG, Jung HS, Shin H. Control of osteogenic differentiation and mineralization of human mesenchymal stem cells on composite nanofibers containing poly[lactic-co-(glycolic acid)] and hydroxyapatite. *Macromol Biosci.* 2010;10:173–182.
42. Lian JB, Stein GS. Concepts of osteoblast growth and differentiation: basis for modulation of bone cell development and tissue formation. *Crit Rev Oral Biol Med.* 1992;3:269–305.
43. Lin L, Chow KL, Leng Y. Study of hydroxyapatite osteoinductivity with an osteogenic differentiation of mesenchymal stem cells. *J Biomed Mater Res A.* 2009;89:326–335.
44. Lv Q, Nair L, Laurencin CT. Fabrication, characterization, and in vitro evaluation of poly(lactic acid glycolic acid)/nano-hydroxyapatite composite microsphere-based scaffolds for bone tissue engineering in rotating bioreactors. *J Biomed Mater Res A.* 2009;91:679–691.
45. Marolt D, Campos IM, Bhumiratana S, Koren A, Petridis P, Zhang G, Spitalnik PF, Grayson WL, Vunjak-Novakovic G. Engineering bone tissue from human embryonic stem cells. *Proc Natl Acad Sci.* 2012;109:8705–8709.
46. Martinez E, Engel E, Planell J, Samitier J. Effects of artificial micro-and nano-structured surfaces on cell behaviour. *Ann Anat.* 2009;191:126–135.
47. Müller P, Bulnheim U, Diener A, Lüthen F, Teller M, Klinkenberg E-D, Neumann H-G, Nebe B, Liebold A, Steinhoff G, Rychly J. Calcium phosphate surfaces promote osteogenic differentiation of mesenchymal stem cells. *J Cell Mol Med.* 2008;12:281–291.
48. Ngiam M, Liao S, Patil AJ, Cheng Z, Chan CK, Ramakrishna S. The fabrication of nano-hydroxyapatite on PLGA and PLGA/collagen nanofibrous composite scaffolds and their effects in osteoblastic behavior for bone tissue engineering. *Bone.* 2009;45:4–16.
49. Pham QP, Sharma U, Mikos AG. Electrospun poly(ε-caprolactone) microfiber and multilayer nanofiber/microfiber scaffolds: characterization of scaffolds and measurement of cellular infiltration. *Biomacromolecules.* 2006;7:2796–2805.
50. Ripamonti U, Crooks J, Kirkbride A. Sintered porous hydroxyapatites with intrinsic osteoinductive activity: geometric induction of bone formation. *South African J Sci.* 1999;95:335–343.
51. Saito E, Liao EE, Hu WW, Krebsbach PH, Hollister SJ. Effects of designed PLLA and 50: 50 PLGA scaffold architectures on bone formation in vivo. *J Tissue Eng Regen Med.* 2013;7:99–111.
52. Salgado AJ, Coutinho OP, Reis RL. Bone tissue engineering: state of the art and future trends. *Macromol Biosci.* 2004;4:743–765.
53. Shao Z, Zhang X, Pi Y, Wang X, Jia Z, Zhu J, Dai L, Chen W, Yin L, Chen H. Polycaprolactone electrospun mesh conjugated with an MSC affinity peptide for MSC homing in vivo. *Biomaterials.* 2012;33:3375–3387.
54. Sikavitsas VI, Bancroft GN, Mikos AG. Formation of three-dimensional cell/polymer constructs for bone tissue engineering in a spinner flask and a rotating wall vessel bioreactor. *J Biomed Mater Res.* 2002;62:136–148.
55. Skardal A, Sarker SF, Crabbé A, Nickerson CA, Prestwich GD. The generation of 3-D tissue models based on hyaluronan hydrogel-coated microcarriers within a rotating wall vessel bioreactor. *Biomaterials.* 2010;31:8426–8435.
56. Thibault RA, Mikos AG, Kasper FK. Protein and mineral composition of osteogenic extracellular matrix constructs generated with a flow perfusion bioreactor. *Biomacromolecules.* 2011;12:4204–4212.
57. Vert M, Mauduit J, Li S. Biodegradation of PLA/GA polymers: increasing complexity. *Biomaterials.* 1994;15:1209–1213.
58. Xing Z, Xue Y, Dånmark S, Schander K, Ostvold S, Arvidson K, Hellem S, Finne-Wistrand A, Albertsson AC, Mustafa K. Effect of endothelial cells on bone regeneration using

poly(L-lactide-co-1,5-dioxepan-2-one) scaffolds. *J Biomed Mater Res A*. 2011;96:349–357.
59. Yang X, Wang D, Hao J, Gong M, Arlet V, Balian G, Shen FH, Li XJ. Enhancement of matrix production and cell proliferation in human annulus cells under bioreactor culture. *Tissue Eng A*. 2011;17:1595–1603.
60. Yu X, Botchwey EA, Levine EM, Pollack SR, Laurencin CT. Bioreactor-based bone tissue engineering: The influence of dynamic flow on osteoblast phenotypic expression and matrix mineralization. *Proc Natl Acad Sci U S A*. 2004;101:11203–11208.
61. Zandi M, Mirzadeh H, Mayer C, Urch H, Eslaminejad MB, Bagheri F, Mivehchi H. Biocompatibility evaluation of nano-rod hydroxyapatite/gelatin coated with nano-HAp as a novel scaffold using mesenchymal stem cells. *J Biomed Mater Res A*. 2010;92:1244–1255.